

Enhanced Cycling Stability of Lithium-Rich Cathode Materials Achieved by in-situ Formation of LiErO₂ Coating

Zhicheng Wei,^[a] Da Zhang,^[a] Jianjian Zhong,^[a] Chaoliang Zheng,^[a] Jiameng Feng,^[a] and Jianling Li*^[a]

Lithium-rich manganese-based cathode materials are considered ideal for the next-generation lithium-ion power batteries due to their high specific capacity. However, their widespread commercial deployment has received serious limitations, such as low initial coulombic efficiency (ICE), severe voltage and capacity degradation. To solve these issues, the surface of Li-rich layered oxide (LLO) material is uniformly coated with a layer of ternary lithium-rare earth oxides LiErO₂ by synchronous lithium strategy. The LiErO₂-coated material exhibits higher capacity retention of 83.79% with 182.7 mAh g⁻¹ compared with that of the pristine material, which retained 60.54% with 144.1 mAh g⁻¹ after 200 cycles at 0.5 C. The excellent electro-

chemical performance is owing to the high Li⁺ conductivity of the LiErO₂ coating which enhanced the lithiation kinetics of the material, and X-ray photoelectron spectrometer (XPS) results indicate coating layer has abundant oxygen vacancies that facilitate reversible redox processes of oxygen. Meanwhile, the results of high resolution transmission electron microscope (HRTEM) and XPS analyses of the materials after cycling shows the uniform coating can suppress the side reactions between the electrode and electrolyte during long-term cycling, reduce the phase transition of the surface structure, and enhance interfacial stability. This work provides innovative ideas for the design of lithium-rich cathode materials.

Introduction

Due to the advantages of high energy density, long service life, good safety performance and environmental friendliness, lithium-ion batteries have become the primary choice for green batteries.^[1] However, with the continuous improvement of the battery specific energy index, the traditional lithium-ion batteries are gradually unable to meet the new demand. To further obtain batteries with higher energy density than traditional batteries, the pursuit of high-specific capacity cathode materials has become the focus of current research.^[2] Lithium-rich manganese-based cathode materials are composed of layered LiMO₂ (M=Co, Ni, Mn, etc.) and Li₂MnO₃, which exhibit the advantages of superior specific capacity (>250 mAh g⁻¹), high operating voltage (>3.5 V) and high safety, and have become a promising cathode material for lithium-ion batteries.^[3]

The superior specific capacity of lithium-rich cathode materials mainly derives from the charge compensation of anions, besides the redox of the transition metal ions during the initial charge.^[4] Unfortunately, the migration and dissolution of the transition metal ions lead to the local phase transformation from a layered structure to a rock salt phase on the material surface during the cycling process, which not only

reduces the electrochemical activity of the material, but also increases the electrochemical impedance, further triggering capacity attenuation and voltage decay.^[5] In addition, a large number of side reactions between the electrode interface and the electrolyte further deteriorate the structure on the surface of the material. The structural deterioration of the material will gradually extend from the surface to the interior, eventually exacerbating the performance decay of the material.^[6]

To solve the above problems, a variety of modification means have been proposed, such as element doping,^[7] surface modification^[8] and pretreatment,^[9] etc. Among them, surface coating has become one of the most effective modification methods to improve the interfacial stability of the material. The application of electrochemically inactive compounds coating (e.g., metal oxides,^[10] fluorides,^[11] and phosphates^[12]) to construct an isolation layer at the interface between the material and electrolyte can effectively reduce the side reactions at the interface and avoid the corrosion of the material by HF and the release of oxygen. It also inhibits the transformation from the surface layered structure to spinel phase, improving the structural stability during cycling.^[13] However, the diffusion of lithium ions at the electrode interface is affected due to the low ionic conductivity of the passivated layer, further leading to an increase in the irreversible capacity of the material and affecting the rate performance.

Rare earth elements are often used as cladding in the form of binary oxides,^[14] and ternary lithium-rare earth oxides as cladding materials are less studied at present. The element Er often exists in the form of Er₂O₃.^[15] It is shown that high-temperature calcination in an atmosphere rich in Li and O will eventually produce LiErO₂.^[16] LiErO₂ has a unique crystal structure which facilitates Li⁺ transport and is expected to be a

[a] Z. Wei, D. Zhang, J. Zhong, C. Zheng, J. Feng, Prof. J. Li
State Key Laboratory of Advanced Metallurgy
School of Metallurgical and Ecological Engineering
University of Science and Technology Beijing
Beijing 100083 (China)
E-mail: lijianling@ustb.edu.cn

 Supporting information for this article is available on the WWW under
<https://doi.org/10.1002/batt.202200568>

cladding material for new lithium-rich manganese-based cathode materials.

Conventional cladding methods such as atomic layer deposition(ALD),^[17] mechanical mixing,^[18] and sol-gel methods^[19] are all the post-processing of the original material. As the most widely used method, the mechanical mixing method mainly grows the cladding layer on the surface of the material through high-energy ball milling, followed by the heat treatment. This method not only has a tedious experimental procedure, but also fails to achieve a low-thickness, uniform coating on particle surfaces due to agglomeration, random distribution of material and irregularity of particle shapes, etc.

In this paper, a ternary lithium-rare earth oxides LiErO_2 coating was constructed *in situ* on the lithium-rich cathode material surface via a synchronous lithium strategy. Er^{3+} was added during the preparation of material precursors by the co-precipitation method. Since there is a larger difference in ionic radius between the Er element and Ni, Co, Mn and O elements, Er cannot occupy the crystal sites of the material. Therefore, it can only be precipitated on the surface of the material, and finally the cathode material with a uniform LiErO_2 covering is obtained. The LiErO_2 coating can effectively reduce the direct contact between electrode and electrolyte, while the great Li^+ transport performance enhances the lithium-ion diffusion ability of the composite. The morphological, structural and electrochemical properties of this cladding layer on the material were systematically investigated by TEM, CV and EIS. The results show that LiErO_2 coating plays an important role in reducing the structural deterioration of the material surface and suppressing the voltage decay and capacity attenuation during cycling. In addition, the rate performance has been significantly improved. This work provides a novel direction which enhancing the performance of lithium-rich layered oxides using surface coating strategies.

Results and Discussion

Figure 1(a) shows the synthetic schematic illustration for the *in-situ* synthesis of LiErO_2 coatings via the synchronous lithium strategy. Since the radius of Er^{3+} is much larger than that of the transition metal, the addition of Er element in the co-precipitation process cannot easily enter the transition metal layer.^[15] $\text{Er}_2(\text{SO}_4)_3$ solution was added dropwisely after the completion of the transition metal ion reaction, and Er^{3+} formed a precipitation layer on the particle surface under alkaline conditions, and precursors wrapped by $\text{Er}(\text{OH})_3$ were obtained. Finally, LiErO_2 -coated cathode material was obtained after the calcination with $\text{LiOH}\cdot\text{H}_2\text{O}$ at elevated temperature. Figure 1(b) demonstrates that LiErO_2 possesses a unique crystal structure which contributes to the rapid transportation of Li^+ . The coating provides good lithium-ion diffusion kinetics while protecting the layered structure, ensuring structural stability during cycling.

The XRD patterns of the original material and LiErO_2 -coated materials with different contents are shown in Figure 2(a). It can be clearly seen that the main diffraction peaks of all materials are recognizable as the $\alpha\text{-NaFeO}_2$ type hexagonal structure of the space group $R\bar{3}m$, and the additional diffraction peaks appearing at $20^\circ\text{--}25^\circ$ can be indexed to the LiMn_6 superlattice structure of the Li_2MnO_3 with $C2/m$ space group. All materials have some degree of crystallinity verified by the sharp diffraction peaks. By comparing the XRD spectra more carefully, in the XRD spectrum of the modified material, four new diffraction peaks appear at 22° , 33° , 41° and 47° , corresponding to the (110) , $(20\bar{2})$, (121) and (031) crystal plane of the LiErO_2 phase. The XRD data of LiErO_2 are shown in Figure S1. The refinement results for each material are shown in Figure S2. The degree of mutual occupation of Li and TM in the material can be judged by comparing the intensity of the (003) peak with that of the (104) peak.^[20] The position of the crystal plane observed from the $[010]$ crystal band axis is shown in Figure 2(b), when TM occupies the Li position, the intensity of (003) will decrease and the intensity of (104) will increase.



Figure 1. a) Schematic diagram of LiErO_2 coating synthesis on LLO surface by simultaneous lithiation. b) Crystal structure diagram of LiErO_2 phase and layered phase.

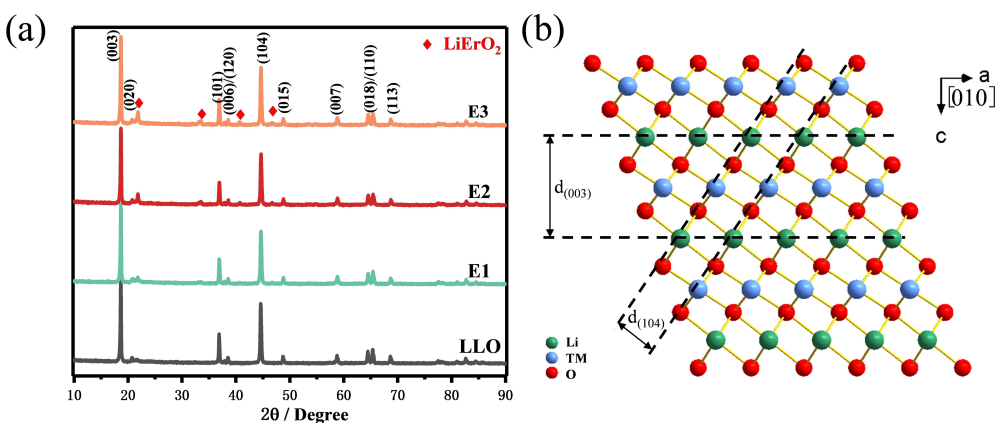


Figure 2. a) XRD patterns of LLO, E1, E2 and E3. b) Schematic of the crystal structure of the layered material.

The smaller the ratio of $I_{(003)}/I_{(104)}$, the higher the degree of mixing represented and the lower the structural stability of the material. The values of $I_{(003)}/I_{(104)}$ of the LLO and E1, E2, E3 materials are 1.436, 1.477, 1.464 and 1.442, respectively, it suggests that cladding material with lower Li and TM confusion and higher lithium ion diffusion ability.

Table 1 shows the crystal structure details analyzed by XRD Rietveld refinements. It is worth noting that the lattice constants a and c of E1, E2 and E3 materials do not change significantly, indirectly verifying that the Er element is not doped into the lattice interior. Interestingly, the values of c/a increased for all modified materials, indicating all exhibit more complete layered structures.^[20]

To analyze the change of particle morphology and size, scanning electron microscopy tests were performed for the modified material and LLO. As can be seen in Figure 3(a), the original material show a smooth surface but without a regular shape, and the particle size is between 100–200 nm. The size and morphology of the modified materials did not change significantly. Figure 3(b) corresponds to the E1 sample, some tiny particles can be seen on the surface of E1 material, which are tentatively estimated to be LiErO₂ particles. The inability to form a complete coating on the surface of the original material is due to the low content of LiErO₂. Figure 3(c) shows the electron microscopy image of the E2 sample, and it can be clearly observed that the particles have a rough surface, while the particles are closely connected to each other. Figure 3(d) shows the electron microscopy image of E3 sample, it can be easily seen that there are a large number of particles on the surface of the material with obvious agglomeration. Moreover, the cathode material shows unsharp boundaries and nonuni-

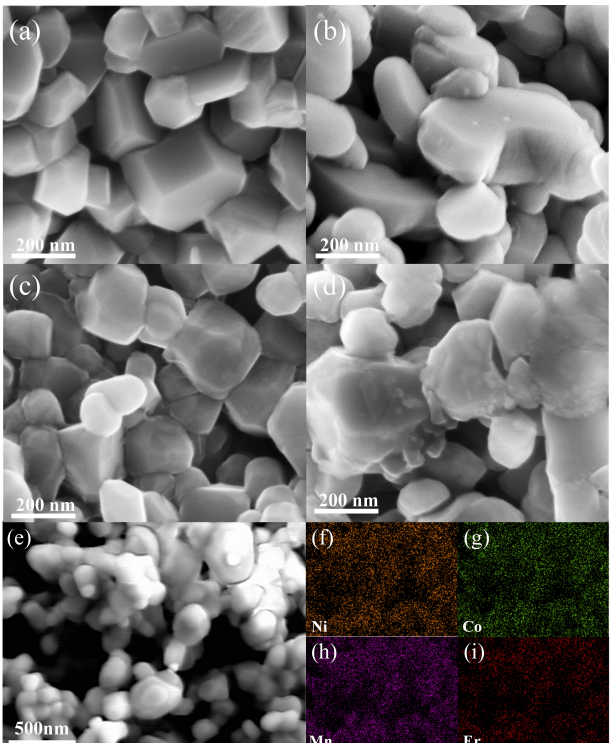


Figure 3. a-d) SEM images of LLO, E1, E2 and E3. e) SEM at higher scale for E2 material. EDS energy spectrum of f) Ni, g) Co, h) Mn, and i) Er.

form particle size. It means that the crystallinity of the material decreases, which will deteriorate the electrochemical performance of the material.

To further analyze the composition of the surface coating of E2 material, a randomly selected region of E2 material is selected for EDS testing. It can be observed from Figure 3(e) that Ni, Co and Mn elements were uniformly distributed within the material without segregation. Meanwhile, the test results appear uniformly present Er elements. Combined with the XRD and SEM test results, it can be tentatively concluded that LiErO₂ is uniformly wrapped on the surface of LLO particles. The significant difference in contrast may be caused by the height difference of the material in the photographed area.

Table 1. Refined data of the lattice parameters and refinement parameters.

Sample	A [Å]	c [Å]	$I_{(003)}/I_{(104)}$	c/a	R_{wp}
LLO	2.8513	14.2444	1.436	4.9957	2.35 %
E1	2.8493	14.2451	1.477	4.9995	3.44 %
E2	2.8494	14.2483	1.464	5.0004	3.59 %
E3	2.8481	14.2486	1.442	5.0028	3.74 %

The transmission electron microscope (TEM) is used to observe the microstructure of the material in more detail. Figure 4(a, b) displays the particle morphology of LLO and E2 materials, respectively, and it can be visibly observed that the particle appearance is basically the same. The partial enlargement of the structure in the yellow box for LLO is clearly shown in Figure 4(c), which shows that uncoated material presents only lattice stripes in one direction, and the clear lattice stripes indicate a perfect crystal structure. The lattice spacing of

0.432 nm is indexed to the (020) crystal plane of the monoclinic phase Li_2MnO_3 component, which is also demonstrated by the fast Fourier transform (FFT) in the inset. And the diagram of the crystal structure for LLO is schematically shown in Figure 4(e). Similarly, Figure 4(d) displays the specific structure characteristic of the material E2. It can be clearly observed that E2 shows lattice fringes in two different directions. The internal lattice fringe with the spacing of 0.409 nm corresponds to the (110) plane of the $\text{C}2/\text{m}$ space group, and the atoms are arranged as shown in Figure 4(f). The lattice stripe with the spacing of 0.209 nm is indexed to the (102) crystal plane of the LiErO_2 phase. Thus, it can be confirmed that LiErO_2 is uniformly coated on the surface of the cathode material. More importantly, the clear lattice stripes inside the E2 material demonstrate that the LiErO_2 coating has no negative impact on the internal structure of the material. According to Figure 4(d), it can be clearly observed that the thickness of LiErO_2 coating on the material surface is about 2–3 nm. The LiErO_2 coating prevents excessive corrosion of the electrode by the electrolyte, while the thin coating thickness has less effect on the charge transfer resistance at the interface between the electrode and the electrolyte.^[21] While the rate performance of the material will be significantly improved based on the high Li-ion conductivity of LiErO_2 .

X-ray photoelectron spectroscopy (XPS) is applied to identify and corroborate the change in the elemental valence of the material before and after modification. According to Figure 5(a, c), the binding energies of Co, Mn and Ni (780.1 eV, 642.4 eV, 854.8 eV) for the modified material hardly change compared with the original material.^[22] It manifests that the valence of the transition metal elements remains stable after modification, suggesting that Er^{3+} does not occupy the sites of transition metals. As shown in Figure 5(d), the peak at 169.3 eV for all modified samples is indexed to the characteristic peak of

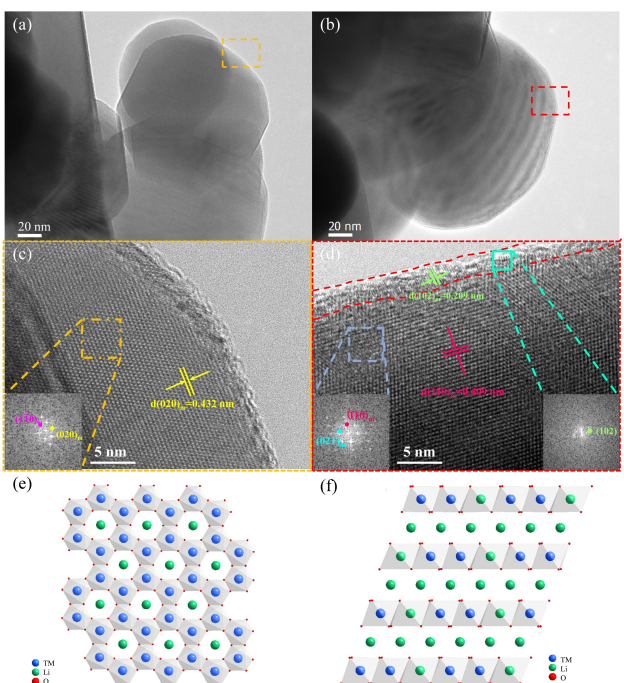


Figure 4. TEM images of a) LLO, and b) E2. HRTEM images of c) LLO and d) E2. e, f) Simulation of the internal crystal structure of LLO and E2 materials.

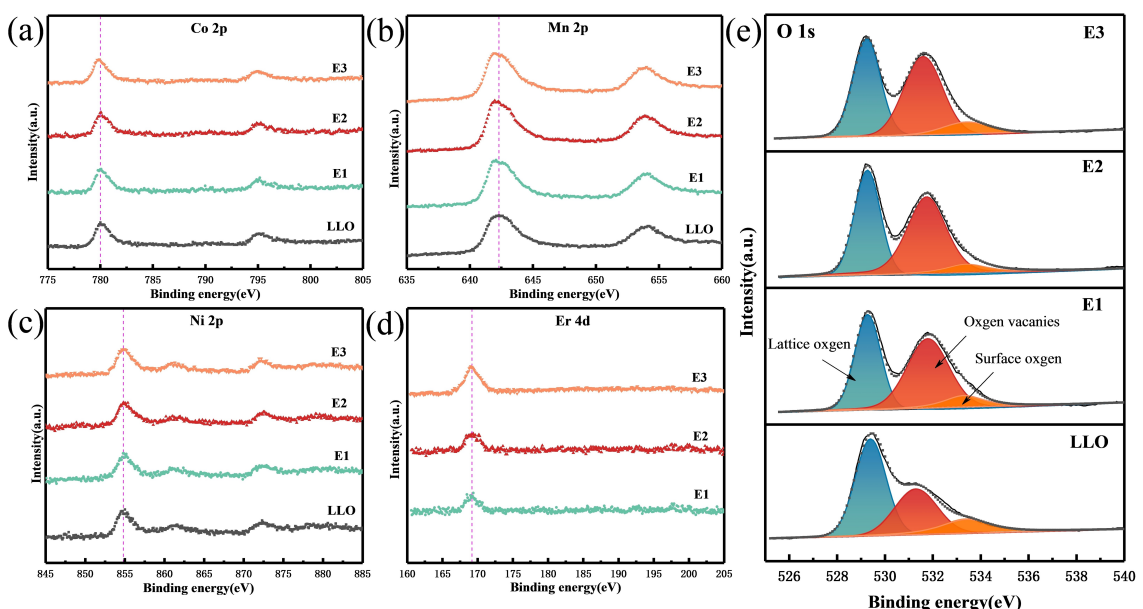


Figure 5. The XPS spectra of LLO and E1, E2, E3: a) Co 2p, b) Mn 2p, c) Ni 2p, d) Er 4d and e) O 1s.

Er 4d, and the peak intensity increases gradually with the increase of the content, which proves the distribution of Er element on the surface of the material.

At the same time, the fitting result for O 1s is shown in Figure 5(e). Generally, the fitted peak at 529.4 eV indicates surface lattice oxygen, and the two fitted peaks at 531.3 eV and 533.4 eV represent oxygen vacancies and surface oxygen, respectively. After modification, the oxygen vacancy content on the surface of the material all increased. It is reasonable to speculate that LiErO₂, which is rich in oxygen vacancies, is attached to the surface of the material. It is widely accepted that oxygen is released from the surface layer of the material to the electrolyte during cycling, which leads to the decomposition of the electrolyte and the corrosion of the material by HF. Oxygen vacancies reduce the formation of highly reactive oxygen radicals and reduce the partial pressure of oxygen on the cathode surface, thus reducing the precipitation of O₂ gas.^[23] The oxygen vacancy-rich LiErO₂ coating can inhibit the release of oxygen and reduce the occurrence of side reactions, which is instrumental in the improvement of cycling stability.

Subsequently, electrochemical tests were performed for all materials. The initial charge and discharge curves of the

materials at 0.05 C are shown in Figure 6(a). All materials exhibit the typical initial charge/discharge curves with no additional plateau. As known to all, the slope region after 3.8 V corresponds to highly reversible oxidation of Ni²⁺ and Co³⁺, with the detachment of lithium ions from the lithium layer.^[24] After charging to 4.45 V, the appearance of the long plateau region corresponds to the activation of the Li₂MnO₃ component with the deeper removal of Li⁺ ions.^[25] Simultaneously, the oxygen anion is involved in charge compensation and finally O₂ is produced and lost. The absence of a plateau region during the next charging process indicates the irreversibility of oxygen loss. The discharge specific capacities of LLO and the LiErO₂-coated materials are 286.4, 279.1, 269.1 and 260.1 mAh g⁻¹, respectively, and the corresponding initial coulombic efficiencies are 79.7%, 79.1%, 81.4%, and 77.2%. The reduction of discharge capacity is ascribed to the consumption of part of the LiOH to generate LiErO₂ in the process of lithiation. The improvement of coulombic efficiency is due to that the increase in oxygen vacancies on the surface reduces the oxygen release and enhances the reversible redox of anions.

To analyze the changes in redox potential for LLO and E2, cyclic voltammetry test is performed. The CV curves for the first

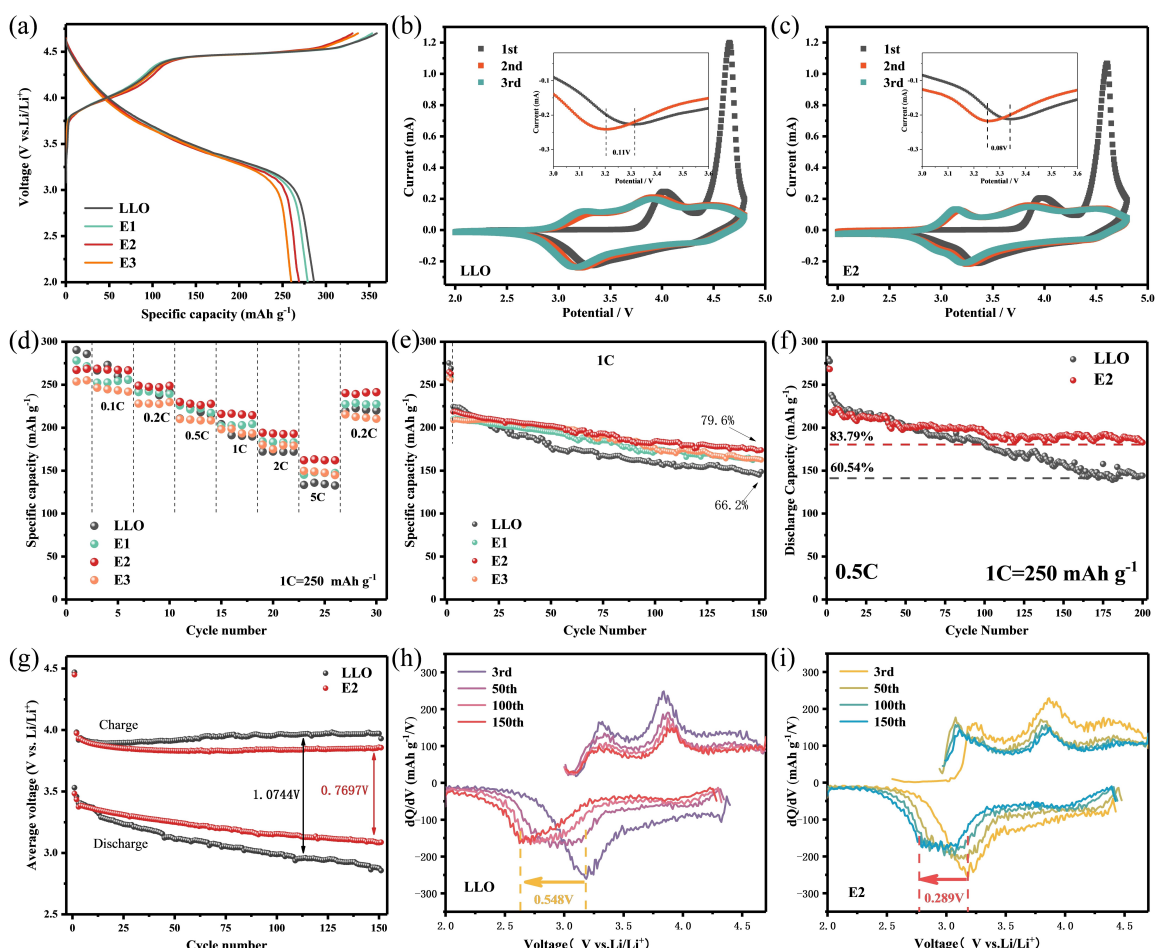


Figure 6. The electrochemical performance of LLO and E1, E2, E3: a) Initial charge/discharge curves, cyclic voltammetry (CV) curves of the material in the first three turns: b) LLO, c) E2. d) Scatter plot of rate performance. e) The cycling performance at 1 C. f) The cycling performance at 0.5 C. g) Average voltage decay of charge and discharge of LLO and E2 materials at 1 C. h and i) Capacity differential curve of LLO and E2 materials at different cycles.

three cycles are shown in Figure 6(b, c). In the black curve (1st cycle), the oxidation peak at 4.0 V corresponds to the oxidation process of Ni^{2+} and Co^{3+} , and the oxidation peak at 4.45 V corresponds to the oxidation process of element O. In the red curve (2nd cycle), the intensity of the oxidation peak at 4.45 V decreases dramatically, further indicating that the oxygen loss is irreversible. During the discharge process, the reduction peaks appearing around 3.3 V represent the reduction reactions of the low-valence transition metal elements, and the reduction peaks around 4.4 V belong to the reduction reactions of the high-valence Ni and Co.^[26] In addition, an oxidation peak appears around 3.2 V at the beginning of the second cycle, corresponding to the involvement of Mn^{3+} in the oxidation. And the oxidation peak of O is missing, which shows that the activation of Li_2MnO_3 component is basically completed. Comparing the first and second CV curves of the LLO and E2, the reduction peak at 3.3 V for E2 material was found to be less shifted, it indicates that the stability of the interface structure is improved and the voltage decay is mitigated. Figure S3 shows the capacity differential curves for LLO and E2. It can be found that the voltage attenuation of E2 material is effectively alleviated compared to LLO. The results are consistent with CV test.

The rate performance of the materials are shown in Figure 6(d). To achieve the purpose of activating the material, each sample is first tested twice at low current density, and then tested at increasing current density from 0.1 C to 5 C and finally back to 0.2 C. At low current densities, the discharge specific capacity of the modified material has a lower value and is not higher than the original material, but the advantages of the modified material gradually emerge with the rise in the current density. The E2 material achieves a discharge specific capacity of 162.1 mAh g^{-1} at 5 C, while the LLO shows capacity of only 134.3 mAh g^{-1} . The improvement in rate performance may be owing to the excellent conductivity of LiErO_2 with its unique crystal structure, while the thin and uniform coating reduces the charge transfer impedance at the interface, thus allowing electrons and Li^+ to shuttle rapidly between the electrode and the electrolyte.

To clarify the influence of LiErO_2 coating on cycling performance, the material was cycled twice at 0.05 C to activate the material, followed by cycling 150 times at 1 C. As shown in Figure 6(e), the E2 material can deliver a specific discharge capacity about 173.9 mAh g^{-1} after 150 cycles with a capacity retention of 79.6%. However, the discharge specific capacity of LLO is about 148.8 mAh g^{-1} and the capacity retention is only 66.2%. Moreover, the E2 material also exhibits good cycling performance at 0.5 C, as shown in Figure 6(f). After 200 cycles, the E2 surprisingly has a specific discharge capacity of 182.7 mAh g^{-1} and exhibits a capacity retention of 83.79%. For uncoated materials, the discharge specific capacity is only 144.1 mAh g^{-1} and the capacity retention rate is as low as 60.54%. Figure 6(g) shows the relationship between average charge-discharge voltage and cycle number. The E2 shows the average discharge voltage attenuation of 0.289 V with a voltage retention of 91.5% after 150 cycles. For the LLO materials, the average discharge voltage decays by 0.548 V with a voltage

retention rate of 83.9%. Furthermore, the average voltage difference value between the charge and discharge for E2 is only 0.7697 V, which is significantly lower than the 1.0744 V for LLO. It illustrates that the good ion conductivity and more smooth charge carrier diffusion channel of LiErO_2 coating can effectively inhibit the polarization of the materials.

The capacity differentiation method can analyze the relationship in depth between the redox reaction and the voltage decay during the cycle, the charge/discharge curves for the 3rd, 50th, 100th and 150th cycles of the materials were calculated as shown in Figure 6(h, i). The generally accepted that the oxidation peaks at 3.3 V, 4.0 V and 4.4 V are assigned to the oxidation of low-valence Mn, high-valence Ni and Co, low-valence Ni and Co, respectively. Meanwhile the reduction peaks at 3.3 V and 4.3 V correspond to reduction reactions with low-valence transition metals, high-valence transition metals and oxygen, respectively.^[27] The reduction curve gradually shifts to lower potentials with cycling, which is attributed to that the material undergoes a continuous transformation from the layered structure to the spinel/rock salt phase during cycling leading to the voltage decay. It is obvious that the offset of the reduction peak for E2 is smaller than that for LLO. It indicates that the voltage decay and voltage hysteresis of E2 material are notably restrained compared with LLO. It is reasonable to speculate that the LiErO_2 coating reduces the contact of the cathode material with by-products and inhibits corrosion on the structure, and thus suppressing the capacity attenuation and voltage decay during cycling, eventually enhancing the electrochemical performance.

During the high voltage charging process of lithium-rich manganese-based cathode materials, a large number of lithium vacancies appear within the transition metal layer as the lithium ions are rapidly stripped out. The presence of vacancies causes a change in the energy level of the surrounding transition metal atoms. The intra-layer migration of transition metals eventually leads to the aggregation of lithium vacancies and thus the generation of O_2 into the electrolyte, and eventually the decomposition of the electrolyte under high pressure produces HF, which seriously affects the structural stability of the material.^[23,28] The results of the pre-cycle XPS showed that the content of oxygen vacancies on the surface of E2 significantly. The main reason for this is that the LiErO_2 coating contains a large number of oxygen vacancies. Through electrochemical performance testing, the E2 material showed the best coulomb efficiency and cycling stability compared to LLO, with a coulomb efficiency of 81.4% in the first cycle and a capacity retention of 79.6% after 150 cycles (1 C). The increase of oxygen vacancies on the surface can reduce the oxygen loss and reduce the erosion of HF to a certain extent, thus inhibiting the phase transition of the surface lamellar structure. It has a certain enhancement on the electrochemical performance of the material.

And the chemical changes on the material surface for LLO and E2 sample after 150 cycles were performed by XPS as shown in Figure 7. From Figure 7(a, c), the peak intensity of the characteristic peaks of Mn and Ni is stronger for the modified sample compared with the original material, indicating that the

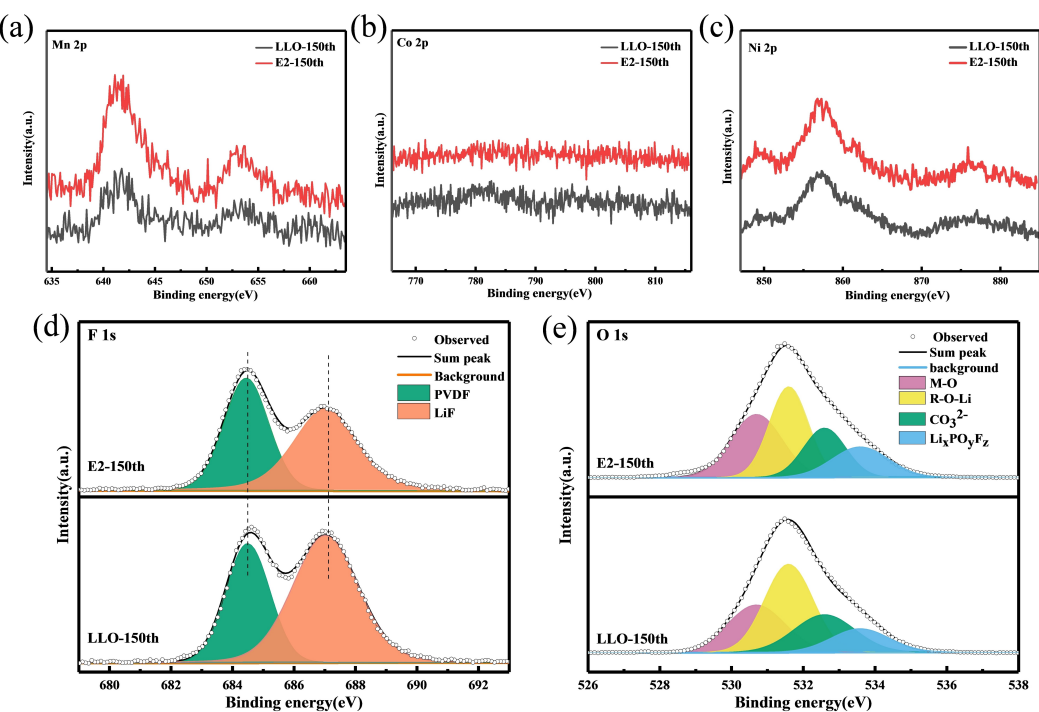


Figure 7. XPS patterns of the surface layers of LLO and E2 materials after 150 cycles: a) Mn 2p, b) Co 2p, c) Ni 2p, d) F 1s, e) O 1s.

LiErO₂ coating protects the electrode/electrolyte interface and inhibits the reduction of transition metals during the cycling. While the Mn 2p_{3/2} peak at 642.1 eV shifts to a lower binding energy after cycling, and the shoulder peak of Mn³⁺ is gradually obvious, indicating a gradual increase in Mn³⁺ content and the generation of spinel-like phase, which eventually leads to the performance deterioration. As shown in Figure 7(b), the Co 2p_{3/2} peak at 780.1 eV almost disappeared after cycling for both the original and modified materials, which is mainly due to the continuous migration of Co elements from the surface to the interior of the particles with the cycling.

The fitted data for the F element are shown in Figure 7(d). The fitted peak appearing at 684.5 eV belongs to the C–F bond, which mostly originates from PVDF in the adhesive. And the fitted peak at 687.2 eV is associated with Li–F. The emergence of LiF is mainly due to the reaction between HF and Li₂O during the cycling process. The area of the LiF peak is significantly reduced in the E2 material, indicated that E2 material produces a thinner SEI film than LLO materials. The analysis of O 1s spectra is shown in Figure 7(e). In general, the binding energies at 530.7, 531.6, 532.6 and 532.6 eV correspond to M–O, R–O–Li, CO₃²⁻ and R–O–Li bonds, respectively. It is found that the characteristic peak area of the M–O bond in the E2 increases significantly, while the peak area of R–O–Li bond changes in the opposite way. It can be speculated that the modified material possesses a thinner cathode-electrolyte interface (CEI) film.^[29] Overall, the coating of LiErO₂ plays a significant role in protecting electrodes and suppressing interfacial side reactions.

TEM testing of LLO and E2 materials after cycling to visualize the protection effect of LiErO₂ coating. As shown in Figure 8(a), it is found that the layered structure of the LLO

material surface structure has been completely destroyed, and the surface covered with spinel phase, disordered rock salt phases and lattice defects. Because the exposed surface of the material has immediate contact with the electrolyte, the corrosion at high voltage is so severe that the laminar structure gradually changes to the electrochemically inactive phase, so the structure changes, which causing performance degradation.^[30] The modified material after cycling is shown in Figure 8(b), it is found that the E2 material keeps a more obvious laminar structure with clear lattice stripes. The lattice stripes of 0.491 and 0.260 nm correspond to the (001) crystal plane of the monoclinic phase and (220) of the spinel phase, respectively. The absence of rock salt phase indicates that the surface structure is slightly deteriorated, the crystal structure is preserved more completely and the lithium ion diffusion channels are well preserved. It is reasonable to assume that the LiErO₂ coating effectively isolates the cathode from the electrolyte, which successfully protect materials from HF corrosion, reduce generation of electrochemically inactive NiO phase, inhibiting the structural degradation and the structural stability has been significantly improved.

The galvanostatic intermittent titration technique (GITT) is a method to effectively analyze the Li⁺ diffusion coefficient (D_{Li^+}). The test results of the modified material and the original material after cycling are shown in Figure 9(a, b). After 150 cycles, the modified material still exhibits higher values compared to the original material, indicating that the modified material undergoes less side reactions with the electrolyte and maintains a more complete layered structure. From Figure 9(b), the advantage is more obvious in the region below 3.2 V, proving that the modification greatly reduces the polarization

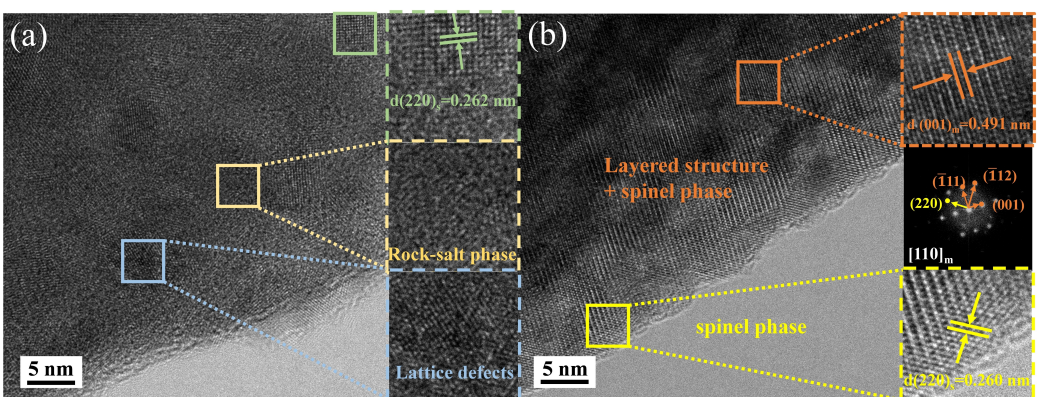


Figure 8. HRTEM plots of a) LLO and b) E2 after 150 cycles.

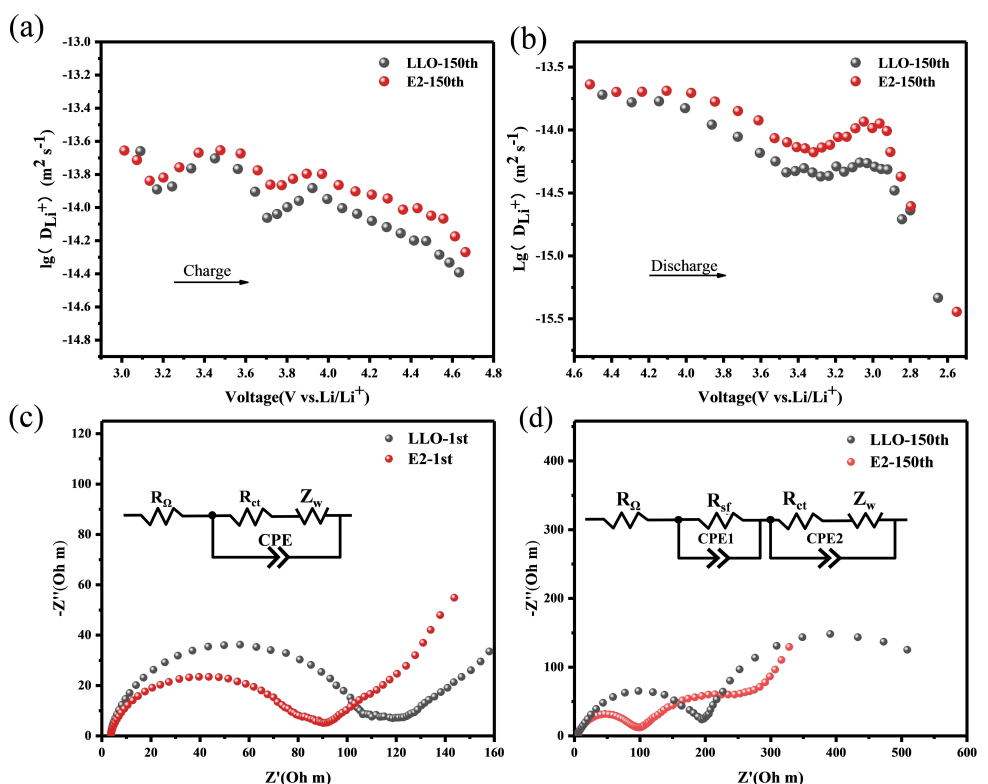


Figure 9. Calculated results from GITT's test data of LLO and E2 materials: a) Charging process after cycling, b) discharging process after cycling. Electrochemical impedance spectra of LLO and E2 materials: c) 1st cycle and d) 150th cycle.

of the material, while increasing medium discharge voltage of the material.

In addition, the difference in the lithium-ion diffusion process between the coated and pristine electrodes has been revealed by electrochemical impedance spectroscopy (EIS). Figure 9(c, d) shows the Nyquist diagram and equivalent circuit of the material before and after cycling. The impedance diagram after 150 cycles consists of two semicircles, where the semicircle in the high-frequency region represents the Li^+ in SEI film transport impedance (R_{sf}), the half-circle in the mid-high frequency region represents the charge transfer impedance (R_{ct}), and the sloping line in the low frequency region

generally represents the transfer impedance of Li^+ within the particle (Warburg impedance). In the impedance plot of the first cycle, only the half-circle of the charge transfer impedance exists because the SEI film has not yet been formed. The fitted data are shown in Table S2. The results before cycling show that the R_{ct} of the LiErO_2 -coated material is significantly lower than that of LLO, which is due to the tighter connection between the particles. After 150 cycles, the R_{sf} of the original material increased by 187.4 Ω compared with only 88.0 Ω of E2, indicating that the LiErO_2 coating may considerably limit the side reactions occurring on the surface of the cathode material, thus inhibiting the SEI film at the interface. Clearly,

modified materials still present a lower R_{ct} . The increase of R_{ct} is related to the phase change during the cycling, indicating that material undergoes less phase transformation. These results confirm that LiErO₂ can effectively inhibit layered structural deterioration of lithium-rich cathodes and improve the cycling stability.

Conclusion

In this paper, a layer of LiErO₂ coating is successfully applied to improve the stability and electrochemical performance of lithium-rich layered oxides by the simultaneous lithiation method. It has been discovered that LiErO₂ coating can enhance the multiple electrochemical performances of the material. Compared with the pristine material, the LiErO₂-coated material exhibits less voltage decay and higher cycling stability, with the voltage retention increasing from 83.9% to 91.5% and the capacity retention increasing from 66.2% to 79.8% after 150 cycles at 1 C. And the material achieved a high capacity of 162.1 mAh g⁻¹ at 5 C. The excellent electrochemical properties of the material are attributed to that the LiErO₂ coating can prevent the corrosion of HF on the electrode, reduce the dissolution of transition metals, and alleviate the deterioration of the surface layered structure, thereby enhancing the cyclic stability of the material. In addition, the surface coating has abundant oxygen vacancies can inhibit oxygen production and reduce electrolyte decomposition and the coating possesses a high lithium-ion conductivity, which can improve the diffusion efficiency of lithium ions between the particles and the electrolyte, further enhancing the rate performance. This work provides a new idea for constructing stable interfacial layers at the interface of lithium-rich layered oxides using ternary lithium oxides LiRO₂ (R=rare earths).

Experimental

Synthesis of samples

The original material Li_{1.2}Mn_{0.54}Ni_{0.13}Co_{0.13}O₂ was synthesized via a simple co-precipitation method. NiSO₄·6H₂O, CoSO₄·7H₂O and MnSO₄·H₂O were dissolved by adding deionized water in the molar ratio of 0.13:0.13:0.54 to obtain a 2 mol L⁻¹ sulfate solution, ammonia was added to deionized water together with KOH to obtain a lye solution with 4 mol L⁻¹. After that, the sulfuric acid solution was added to the reactor together with the lye, and the transition metal elements were allowed to precipitate at 60 °C and pH=12. Aging time of 5 min is used to obtain primary pellets. And the precursors were obtained by filtration and drying. The precursors were then ground well with LiOH·H₂O (5% excess), calcined at high temperatures, holding at 450 °C for 5 h and calcining at 900 °C for 18 h at a heating rate of 5 °C min⁻¹. Finally, the product was cooled to room temperature to obtain the targeted Li-rich layered oxides (LLO). To obtain LiErO₂-coated materials, additional Er₂(SO₄)₃ solutions of different molar ratios (0.01, 0.02 and 0.03) were added during the co-precipitation experiment. Finally, the materials with different LiErO₂ coating amounts were obtained and marked as E1, E2 and E3.

Material characterizations

Analysis of the crystal structure composition of the material was carried out using X-ray diffraction (XRD) (PANalytical, PW 3040-X'Pert Pro) with a Cu K_α radiation source in the range of 10°–90° at a rate of 2° min⁻¹. FESEM (Zeiss SUPRATM55) was used to observe the microscopic morphology of the material before and after treatment. The surface structure of the material was observed and analyzed in more detail using transmission electron microscopy (TEM, JEOL-JEM 2100). The composition and valence of the elements were verified by X-ray photoelectron spectrometer (XPS) (Thermo Scientific K-Alpha+).

Electrochemical techniques

The electrode sheet was mainly composed of active material (75 wt %), Super P (15 wt%), and PVDF (10 wt%) with an active material loading of about 2–3 mg. First, the active material was mixed and ground with Super P for 20 min. After that, the bonding agent (PVDF dissolved in NMP) was added dropwisely under continued grinding for 8 min. The mixed slurry was then evenly applied on the aluminum foil, and vacuum-dried at 120 °C for 8 h. It was cut into electrode pieces with a diameter of 12 mm. A 2032 type button cell was assembled in a glove box filled with argon gas. The negative electrode was lithium metal, the main composition of the electrolyte was 1 M LiPF₆/EC:DMC (1:1), and the diaphragm was Celgard 2500 separators. Constant current charge/discharge testing of batteries in the voltage range of 2.0 V and 4.7 V using the LAND CT2001 A instrument. The test current density was expressed in C, 1 C=250 mAh g⁻¹. Electrochemical impedance spectra (EIS) were recorded for cells at a charging voltage of 4 V using a VMP2 electrochemical workstation (Princeton Applied Research VersaSTAT3). The test frequency was 10 MHz~10 mHz and the amplitude was 5 mV. The galvanostatic intermittent titration technique (GITT) was used to measure the Li electrochemical diffusion coefficient. The battery was first charged at constant current (25 mAh g⁻¹) for 20 mins, followed by an open-circuit resting period of 80 min.

Acknowledgements

This work is financially supported by the National Natural Science Foundation of China (Grants 51972023).

Conflict of Interest

The authors declare that they have no known competing financial interests or personal relationships that could have appeared to influence the work reported in this paper.

Data Availability Statement

The data that support the findings of this study are available from the corresponding author upon reasonable request.

Keywords: cycling stability · lithium-ion battery · lithium-rich layered oxide · surface coating · ternary lithium-rare earth oxide

- [1] a) X. Zeng, M. Li, D. Abd El-Hady, W. Alshitari, A. S. Al-Bogami, J. Lu, K. Amine, *Adv. Energy Mater.* **2019**, *9*, 1900161; b) W. Li, B. Song, A. Manthiram, *Chem. Soc. Rev.* **2017**, *46*, 3006–3059.
- [2] R. Schmuck, R. Wagner, G. Hörpel, T. Placke, M. Winter, *Nat. Energy* **2018**, *3*, 267–278.
- [3] a) M. Li, J. Lu, Z. Chen, K. Amine, *Adv. Mater.* **2018**, *30*, 1800561; b) W. He, W. Guo, H. Wu, L. Lin, Q. Liu, X. Han, Q. Xie, P. Liu, H. Zheng, L. Wang, X. Yu, D. L. Peng, *Adv. Mater.* **2021**, *33*, 2005937; c) H. Yu, H. Zhou, *J. Phys. Chem. Lett.* **2013**, *4*, 1268–1280.
- [4] a) J. Xu, M. Sun, R. Qiao, S. E. Renfrew, L. Ma, T. Wu, S. Hwang, D. Nordlund, D. Su, K. Amine, J. Lu, B. D. McCloskey, W. Yang, W. Tong, *Nat. Commun.* **2018**, *9*, 947; b) T. Liu, J. Liu, L. Li, L. Yu, J. Diao, T. Zhou, S. Li, A. Dai, W. Zhao, S. Xu, Y. Ren, L. Wang, T. Wu, R. Qi, Y. Xiao, J. Zheng, W. Cha, R. Harder, I. Robinson, J. Wen, J. Lu, F. Pan, K. Amine, *Nature* **2022**, *606*, 305–312; c) H. Wang, J. Lin, X. Zhang, L. Wang, J. Yang, E. Fan, F. Wu, R. Chen, L. Li, *ACS Appl. Energ. Mater.* **2021**, *4*, 6205–6213.
- [5] a) P. Yan, A. Nie, J. Zheng, Y. Zhou, D. Lu, X. Zhang, R. Xu, I. Belharouak, X. Zu, J. Xiao, K. Amine, J. Liu, F. Gao, R. Shahbazian-Yassar, J. G. Zhang, C. M. Wang, *Nano Lett.* **2015**, *15*, 514–522; b) S. Li, S. J. Lee, X. Wang, W. Yang, H. Huang, D. S. Swetz, W. B. Doriese, G. C. O’Neil, J. N. Ullom, C. J. Titus, K. D. Irwin, H. K. Lee, D. Nordlund, P. Pianetta, C. Yu, J. Qiu, X. Yu, X. Q. Yang, E. Hu, J. S. Lee, Y. Liu, *J. Am. Chem. Soc.* **2019**, *141*, 12079–12086.
- [6] a) J. Liu, Z. Bao, Y. Cui, E. J. Dufek, J. B. Goodenough, P. Khalifah, Q. Li, B. Y. Liaw, P. Liu, A. Manthiram, Y. S. Meng, V. R. Subramanian, M. F. Toney, V. V. Viswanathan, M. S. Whittingham, J. Xiao, W. Xu, J. Yang, X.-Q. Yang, J.-G. Zhang, *Nat. Energy* **2019**, *4*, 180–186; b) B.-J. Chae, T. Yim, *J. Power Sources* **2017**, *360*, 480–487.
- [7] K. Zhang, J. Qi, J. Song, Y. Zuo, Y. Yang, T. Yang, T. Chen, X. Liu, L. Chen, D. Xia, *Adv. Mater.* **2022**, *34*, 2109564.
- [8] C. Zheng, Z. Yang, J. Feng, J. Zhong, Z. Wei, J. Li, *J. Mater. Chem. A* **2022**, *10*, 16046–16060.
- [9] J. Zhong, Z. Yang, Y. Liu, J. Li, X. Wang, F. Kang, *Electrochim. Acta* **2019**, *328*, 134987.
- [10] a) X. Zhang, I. Belharouak, L. Li, Y. Lei, J. W. Elam, A. Nie, X. Chen, R. S. Yassar, R. L. Axelbaum, *Adv. Energy Mater.* **2013**, *3*, 1299–1307; b) N. Dannehl, S. O. Steinmüller, D. V. Szabo, M. Pein, F. Sigel, L. Esmezjan, U. Hasenkox, B. Schwarz, S. Indris, H. Ehrenberg, *ACS Appl. Mater. Interfaces* **2018**, *10*, 43131–43143.
- [11] a) X. Ding, Y.-X. Li, F. Chen, X.-D. He, A. Yasmin, Q. Hu, Z.-Y. Wen, C.-H. Chen, *J. Mater. Chem. A* **2019**, *7*, 11513–11519; b) T. Zhao, L. Li, R. Chen, H. Wu, X. Zhang, S. Chen, M. Xie, F. Wu, J. Lu, K. Amine, *Nano Energy* **2015**, *15*, 164–176.
- [12] a) X. Zhang, R. Yu, Y. Huang, X. Wang, Y. Wang, B. Wu, Z. Liu, J. Chen, *ACS Sustainable Chem. Eng.* **2018**, *6*, 12969–12979; b) Z. Wang, R. F. Grant, M. A. Arain, P. Y. Bernier, B. Chen, J. M. Chen, A. Govind, L. Guindon, W. A. Kurz, C. Peng, D. T. Price, G. Stinson, J. Sun, J. A. Trofymow, J. Yeluripati, *Ecol. Modell.* **2013**, *260*, 25–35.
- [13] I. H. Son, J. H. Park, S. Kwon, J. Mun, J. W. Choi, *Chem. Mater.* **2015**, *27*, 7370–7379.
- [14] K. Yang, Y. Liu, B. Niu, Z. Yang, J. Li, *Ionics* **2018**, *25*, 2027–2034.
- [15] S. Zhang, H. Gu, T. Tang, W. Du, M. Gao, Y. Liu, D. Jian, H. Pan, *ACS Appl. Mater. Interfaces* **2017**, *9*, 33863–33875.
- [16] M. Nagura, A. Suzuki, T. Terai, *J. Nucl. Mater.* **2011**, *417*, 1210–1213.
- [17] H. Yu, Y. Gao, X. Liang, *J. Electrochem. Soc.* **2019**, *166*, A2021–A2027.
- [18] a) H. Liu, C. Du, G. Yin, B. Song, P. Zuo, X. Cheng, Y. Ma, Y. Gao, *J. Mater. Chem. A* **2014**, *2*, 15640–15646; b) C. Ghanty, P. P. Dahiya, R. N. Basu, J.-K. Chang, S. B. Majumder, *J. Electrochem. Soc.* **2015**, *162*, A1957–A1965; c) Z. Wang, E. Liu, L. Guo, C. Shi, C. He, J. Li, N. Zhao, *Surf. Coat. Technol.* **2013**, *23*, 570–576.
- [19] D. Wang, T. Xu, Y. Li, D. Pan, X. Lu, Y.-S. Hu, S. Dai, Y. Bai, *ACS Appl. Mater. Interfaces* **2018**, *10*, 41802–41813.
- [20] F. Fu, Y. Yao, H. Wang, G.-L. Xu, K. Amine, S.-G. Sun, M. Shao, *Nano Energy* **2017**, *35*, 370–378.
- [21] U. Nisar, N. Muralidharan, R. Essehli, R. Amin, I. Belharouak, *Energy Storage Mater.* **2021**, *38*, 309–328.
- [22] G. Assat, D. Foix, C. Delacourt, A. Iadecola, R. Dedryvere, J. M. Tarascon, *Nat. Commun.* **2017**, *8*, 2219.
- [23] B. Qiu, M. Zhang, L. Wu, J. Wang, Y. Xia, D. Qian, H. Liu, S. Hy, Y. Chen, K. An, Y. Zhu, Z. Liu, Y. S. Meng, *Nat. Commun.* **2016**, *7*, 12108.
- [24] P. Liu, W. He, Y. Cheng, Q. Wang, C. Zhang, Q. Xie, J. Han, Z. Qiao, H. Zheng, Q. Liu, L. Wang, B. Qu, Q. Luo, Z. Z. Zhu, D. L. Peng, *J. Phys. Chem. Lett.* **2020**, *11*, 2322–2329.
- [25] H. Liu, Y. Chen, S. Hy, K. An, S. Venkatachalam, D. Qian, M. Zhang, Y. S. Meng, *Adv. Energy Mater.* **2016**, *6*, 1502143.
- [26] C. Yang, S. Han, J. Huang, M. Qian, *Mater. Chem. Phys.* **2015**, *149*–*150*, 695–700.
- [27] Z. Yang, J. Zhong, J. Feng, J. Li, F. Kang, *Chem. Eng. J.* **2022**, *427*, 130723.
- [28] F. Li, X. Zhang, J. Lin, J. Ma, S. Zhang, G. Yang, *J. Phys. Chem. C* **2019**, *123*, 23403–23409.
- [29] X.-I. Huang, R.-z. Wang, D. Xu, Z.-I. Wang, H.-g. Wang, J.-j. Xu, Z. Wu, Q.-c. Liu, Y. Zhang, X.-b. Zhang, *Adv. Funct. Mater.* **2013**, *23*, 4345–4353.
- [30] M. Gu, I. Belharouak, J. Zheng, H. Wu, J. Xiao, A. Genc, K. Amine, S. Thevuthasan, D. R. Baer, J.-G. Zhang, N. D. Browning, J. Liu, C. Wang, *ACS Nano* **2013**, *7*, 760–767.

Manuscript received: December 28, 2022

Revised manuscript received: February 16, 2023

Accepted manuscript online: February 19, 2023

Version of record online: March 1, 2023